Temporal variability of nitrous oxide emissions by soils as affected by hydric history

E. Rabot, C. Hénault, Isabelle Cousin

Temporal variability of nitrous oxide emissions by soils as affected by hydric history

E. Rabot, C. Hénault, I. Cousin*

INRA, UR0272, UR Science du Sol, F-45075 Orléans, France

* Corresponding author: isabelle.cousin@orleans.inra.fr

Abstract

Soil water is known to be a key factor for controlling N_2O emissions. The relationship between N_2O emissions and water-filled pore space (WFPS) at hydric equilibrium is often described as exponential, starting at 60% WFPS. Because water in soil is dynamic, however, N_2O emissions should be seen as a dynamic process. In this study, we investigated the role of the soil hydric history on N_2O emissions by varying the intensity and speed of soil drying. We performed a laboratory experiment under non-steady-state equilibrium to control the bottom boundary condition of undisturbed soil cylinders. Three treatments of stepwise drying were performed across the range 0 to −100 cm pressure head in two wetting–drying cycles. Two types of N_2O peaks of the same order of magnitude were detected. A peak appeared within 2 d after rewetting and was related to microbial production processes. The second type of peak was detected within the first two steps of the decreasing pressure head. They occurred during a brief period, an average of 1.6 h after the change in hydric equilibrium, during the phase of steep decline in the soil matric potential. These peaks were induced by diffusion processes, and their intensities were correlated with the amount of water drained. Entrapment of N_2O during the wetting phase and rapid displacement during the drying phase may have occurred. Our results showed that WFPS alone is not able to consistently predict N_2O emissions by soils because production and emission phases must be distinguished.

Abbreviations: BD, bulk density; C1, first wetting–drying cycle; C2, second wetting–drying cycle; SOC, soil organic carbon; VWC, volumetric water content; WFPS, water-filled pore space.

1 Introduction

Nitrous oxide has long been recognized as playing a role in stratospheric ozone depletion and global warming (World Meteorological Organization, 2007; Ravishankara et al., 2009). The increase in the N_2O atmospheric concentration during recent decades, at a rate of approximately 0.2% yr^{-1} (Khalil et al., 2002; Wuebbles, 2009), has made N_2O a matter of concern. Its atmospheric lifetime is approximately 120 yr, and its global warming potential is 300 times higher than that of CO_2 (World Meteorological Organization, 2007). Anthropogenic sources, primarily agricultural practices and their use of fertilizers, are estimated to account for approximately 40% of the N_2O emissions (Denman et al., 2007).

The water in soil is known to be a key factor for controlling N_2O emissions. The water-filled pore space (WFPS), i.e., the proportion of soil pore space filled with water (Linn and Doran, 1984), is often used to explain trends in N_2O emissions by soil. Indeed, WFPS directly determines the soil aerobic conditions because of its role as a barrier to O_2 diffusion (Grundmann and Rolston, 1987), gas diffusion and dissolution (Clough et al., 2005), microbial dynamics (Borken and Matzner, 2009; Kieft et al., 1987; Stark and Firestone, 1995), structural stability (Appel, 1998; Denef et al., 2001; van Gestel et al., 1991), and substrate and microorganism transport (Bateman and Baggs, 2005; Stark and Firestone, 1995). Other indirect effects can also be linked to the water in soil, for example, the inhibition of N_2O reductase by O_2 (Knowles, 1982).

Consequently, water is of primary importance in models that predict N_2O emissions. A response function depending on the soil water content is often implemented in these models. The response function formulation is derived from experiments conducted at hydric equilibrium, i.e., without any macroscopic water flux in the soil. In these experiments, water is added to soil samples to reach a target water content, and the N_2O fluxes are then measured. One widely accepted water content response function has an exponential form starting at approximately 60% WFPS (Beare et al., 2009; Grundmann and Rolston, 1987; Hénault and Germon, 2000). Indeed, these hydric conditions create anaerobic sites that are favorable for denitrification and are not limiting for substrate diffusion or microbial transport (Bateman and Baggs, 2005). Other researchers have suggested a Gaussian relationship between WFPS and N_2O emissions (Castellano et al., 2010; Ciarlo et al., 2007; Davidson et al., 2000), driven by the reduction of N_2O to N_2 at WFPS > 90% and/or by the slower gas diffusion coefficient in soil with high water contents. Because of its shape, and despite numerous attempts to model

N_2O emissions, the high sensitivity of the response function to soil water content is still responsible for prediction errors (Grundmann and Rolston, 1987; Heinen, 2006).

Moreover, Groffman et al. (2009) noted the need for data to predict "hot moments", i.e., high N_2O fluxes produced at the soil surface during brief periods. These fluxes are related to the temporal variability of N_2O emissions. Models often assume that N_2O emissions change immediately with the variation of an environmental factor (Xing et al., 2011), and the temporal variability is usually taken into account in models through fertilization and meteorological input data. However, there is a need to account for the importance of time because soil water is characterized by a dynamic behavior. Thus, a hydric event should be considered to cause direct and also indirect effects with a substantial time lag.

The dynamic nature of N_2O emissions in response to water content changes can be demonstrated by the N_2O peak that is frequently observed from the rewetting of a dry soil, either by rain or as simulated under laboratory conditions (e.g., Groffman and Tiedje, 1988; Sanchez-Martin et al., 2010; Sexstone et al., 1985) as a consequence of the "Birch effect" (Birch, 1958). This phenomenon lasts 1 to 4 d after wetting (Fierer and Schimel, 2002). Some studies have tried to compare the effect of the direction of a hydric change, i.e., wetting or drying. Groffman and Tiedje (1988) reported hysteretic responses in N_2O emissions depending on whether a dry soil was rewetted or a wet soil was gradually dried: a peak appeared after rewetting, while emissions were lowered during desiccation. In addition, Kroeckel and Stolp (1986) recorded N_2O emissions following the rewetting of a dry soil that started at a lower water content compared with the case of the further wetting of an already wet soil. Some researchers have also reported that the N_2O peaks become less intense after several wetting–drying cycles (Borken and Matzner, 2009; Muhr et al., 2008). However, the effects of wetting–drying cycles on biomass and bacterial activity could lead to more contrasting results depending on whether the short or the long term is considered (Fierer and Schimel, 2002). In sum, these findings suggest a change from a static to a dynamic point of view. As highlighted by Groffman and Tiedje (1988), "models of denitrification driven by water content will not be accurate unless they consider the wetting history of the soil."

Because the water in soil plays a key role in N_2O emissions, a detailed understanding of soil water dynamics is required to describe N_2O emissions as a dynamic process. In this study, we attempted to highlight the role of the hydric history on N_2O emissions by applying wetting–drying cycles to soil samples and determining the relative importance of N_2O emissions

during wetting and drying. This study focused on the desaturation period, where we investigated the role of the intensity and the speed of soil drying.

2 Material and methods

2.1 Soil sampling

The study site is a commercial agricultural field covered by wheat (*Triticum aestivum* L.), located near Chartres, in the northwest of France (1.196° N, 48.376° E). It was chosen for the high N_2O emissions recorded in the field (Gu et al., 2011). The soils are classified as Haplic Abeluvisols. Two sets of undisturbed soil cores (15-cm inner diameter by 7-cm height) were collected in January and May 2012 from the surface horizon (1–8 cm). The samples had the following properties: clay, 13.7%; silt, 82.0%; sand, 4.3%; soil pH, 6.0. The soil organic C (SOC) and total N contents are given in Table 1. The average bulk density (BD) of the soil samples was 1.32 ± 0.01 g cm^{-3} in January and 1.37 ± 0.01 g cm^{-3} in May (Table 1). The volumetric water content (VWC) at the sampling time was 37.2 ± 1.5% in January and 36.8 ± 0.7% in May (equivalent to 73.8 ± 2.5 and 76.0 ± 2.4% WFPS, respectively). Samples were conditioned in plastic bags and stored field moist at 5°C. Before the start of the experiments, the samples were trimmed on each end and maintained at 20°C for 24 h.

Table 1. Physical and chemical properties of the study site (initial) and of the soil samples at the end of the experiment.

Sample	Sampling period	Bulk density	Modal pore diameter	Soil organic C	Total N	C/N ratio	NO_3^--N
		g cm^{-3}	µm	—— g kg^{-1} ——			mg kg^{-1}
Initial	Jan.			8.08	0.90	8.98	18.7
Initial	May			9.13	1.10	8.30	22.0
Fast-A	Jan.	1.32	3.10	8.78	1.00	8.78	84.0
Fast-B	Jan.	1.33	3.47	8.78	1.00	8.78	58.0
Fast-C	May	1.33	2.99	9.53	1.10	8.67	46.6
Fast-D	May	1.42	3.21	10.12	1.10	9.20	44.7
Medium-A	Jan.	1.30	3.72	8.26	0.90	9.17	43.1
Medium-B	Jan.	1.34	3.74	9.30	1.10	8.46	49.6
Medium-C	May	1.39	3.21	9.53	1.10	8.67	29.5
Medium-D	May	1.36	3.71	9.36	1.00	9.36	58.4
Slow-A	Jan.	1.28	3.46	7.67	0.90	8.53	38.0
Slow-B	Jan.	1.33	4.10	8.55	1.00	8.55	51.8
Slow-C	May	1.37	3.45	11.57	1.10	10.52	51.7
Slow-D	May	1.33	3.71	10.87	1.10	9.88	48.5

2.2 Experimental setup

2.2.1 Hydric control and monitoring

Our experimental design used a tension table (Eijkelkamp Sandbox, 1.4-m air-entry value), which allows the study of N_2O emissions under a non-steady-state equilibrium near saturation with control of the bottom boundary conditions. A schematic overview of the experimental setup is given in Fig. 1. The tension table uses the principle of hydrostatic equilibrium to apply a target pressure head on a soil core placed on a layer of fine synthetic sand (Kutílek and Nielsen, 1994, p. 73–74). The negative pressure head applied to the bottom boundary of the soil core causes its drainage.

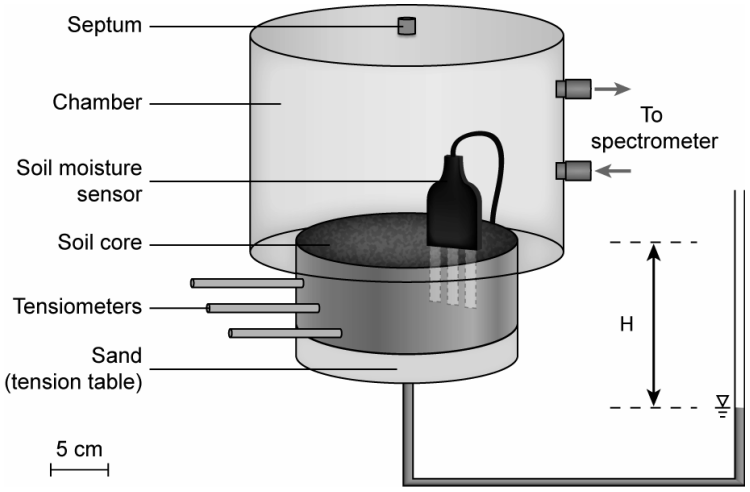

Fig. 1. Schematic overview of the experimental setup for hydric control and N_2O measurements (*H* is pressure head).

The matric potential of the soil cores was monitored with time using three homemade microtensiometers (porous ceramic cup, 20-mm length, 2.2-mm diam., 150-kPa air-entry value) inserted at three depths from the soil surface (3, 4, and 5 cm), thoroughly measured for each sample. The VWC was monitored with a soil moisture sensor (5TE, Decagon Devices) calibrated to assume an accuracy of 2% VWC (Decagon Devices, 2010). The temperature was also recorded at the soil surface by the soil moisture probe. The experiment was conducted under laboratory conditions, with the temperature ranging between 20 and 21°C. Data were recorded every 10 min with a datalogger (CR1000, Campbell Scientific). The calibration of the soil moisture probe was performed under the same conditions as our experimental setup (i.e., wetting solution, range of soil moisture, insertion of the probe, room temperature) on three undisturbed soil samples from the study site. The soil samples were first gradually

saturated by adding solution from the bottom. They were then freely drained while the water content was controlled gravimetrically.

2.2.2 Wetting and drying cycles

Wetting–drying cycles using a KNO_3 solution were performed on each sample. Given that we worked in the near-saturation range, which is a level of water content that is typically involved in the denitrification process (Mathieu et al., 2006), we used NO_3 as the substrate of N_2O production. The KNO_3 solution was prepared with deaired water to prevent air bubble formation. Its concentration (4.1×10^{-2} mol N L^{-1}) was assumed to be large enough so that it was not a limiting factor for N_2O emissions (Hénault and Germon, 2000).

Two wetting–drying cycles were performed on each sample to simulate a water table fluctuation in the soil cores (the first cycle is referred to as C1, and the second cycle is referred to as C2). The zero pressure reference level was the cylinder surface, and the initial water content in each soil sample was its water content at sampling. First, the level of the KNO_3 solution was raised to 1 cm below the top of the soil cores to allow the samples to saturate for 4 d (C1 wetting phase). Raising the solution level from the bottom allowed quasi-saturation of the soil sample by avoiding air entrapment. Drying was then performed stepwise by applying a decreasing pressure head level once a day across the range 0 to −100 cm (C1 drying phase). A second cycle of saturation (C2 wetting phase) and desaturation (C2 drying phase) similar to the C1 cycle was then performed. Evaporation was prevented by keeping a chamber closed above the soil surface.

Three types of wetting–drying cycles were applied to study the effect of the intensity of a pressure head decrease (Table 2). The cycles varied by the number of water pressure head steps needed to reach the maximum −100 cm step. The cycles are hereafter referred as the Fast treatment (three values of pressure head), Medium treatment (four values), and Slow treatment (six values), and they lasted for 12, 14, and 18 d, respectively. These variations in the pressure head are typical of those measured in the field during winter (data not shown). For each treatment, the beginning of a cycle was (i) saturation up to 0 cm and (ii) drainage down to −7 cm to ensure that all the samples experienced the same hydric history before applying larger pressure heads. This is a method of addressing the known heterogeneity in N_2O emissions by fixing at least the recent soil hydric history.

Table 2. Treatments of decreasing pressure heads (one cycle). The reference level for zero pressure is the cylinder surface.

Treatment	Pressure heads applied successively
	cm water column
Fast	0, −7, −100
Medium	0, −7, −50, −100
Slow	0, −7, −25, −50, −75, −100

2.2.3 Gas measurements

The cover of the tension table was modified to fit airtight chambers over the soil cores. Leaks in the chambers were tested daily by adding 5 mL of the inert gas krypton to the headspace. Gases were sampled for krypton measurements in evacuated vials, and its concentration was determined by gas chromatography (μGC Gas Analyzer T-3000, SRA Instruments). Nitrous oxide emissions were monitored by infrared correlation spectroscopy (Model 46i, Thermo Scientific) from the beginning of the experiment. The emissions were measured three to eight times a day for 30-min periods, and the concentration value was recorded every minute. Nitrous oxide fluxes were then calculated linearly from the observed change in concentration during 10 min for the first 20 min after the chamber was closed. The chambers were removed before each measurement to restore the atmosphere to ambient concentrations of gases. The possible N_2O production by the sand of the tension table was also evaluated by regularly sampling gases above areas of the tension table that were not covered by soil cores and analyzing them with gas chromatography. Throughout the experiments, the emissions by the sand were considered to be negligible.

2.2.4 Soil physical and chemical characterization

At the end of the experiment, the soil cores were disrupted and oven dried (48 h at 105°C) to determine their BD and porosity, assuming a particle density of 2.65 g cm^{-3}. The WFPS was then calculated as the ratio between the VWC and porosity (Linn and Doran, 1984). The water outflow during the drying phase was determined from the soil moisture sensor data. The characterization of the pore size distribution of the soil samples in the pore diameter range 430 to 0.006 μm was performed by Hg intrusion porosimetry (AutoPore IV 9500, Micromeritics) on oven-dried aggregates of approximately 1 cm^3. Two replicates for each soil core were measured. At a given pressure head step value, the maximum water-filled pore radius (r) was derived from the Jurin equation:

$$r = \frac{2\sigma\cos(\gamma)}{\rho g|h|} \quad [1]$$

where σ is the surface tension of water at 20°C, γ is the contact angle of water at 20°C, ρ is the density of water, *g* is the gravitational acceleration, and *h* is the soil matric potential recorded at a given pressure head.

The soil NO_3 content was determined by colorimetric analysis (Hach Lange, DR 2800) after the extraction from an 8-g soil sample using 0.5 mol L^{-1} K_2SO_4. Total N was measured by the Dumas method, and SOC was measured by sulfochromic oxidation. Analyses were performed before (for each of the sampling periods) and after the experiment on the tension table.

2.3 Data analyses

Cumulative N_2O fluxes were calculated by linearly interpolating the N_2O flux values that were recorded with time, then integrating the area under the curve (Castellano et al., 2010; Dobbie et al., 1999).

Due to the discontinuity in N_2O emission measurements, the maximum intensity of emissions was not always captured during our experiments. We then analyzed the contribution of each pressure head step to the global N_2O emissions by calculating the slope of the N_2O flux curve just after the application of a pressure head step:

$$a_h = \frac{F(t_h) - F(t_{0,h})}{t_h - t_{0,h}} \quad [2]$$

where *a* is the N_2O flux slope (mg N m^{-2} d^{-2}), *F* is the N_2O flux (mg N m^{-2} d^{-1}), *h* is the pressure head step, $t_{0,h}$ is the time of the first flux measurement of a given pressure head step (d), and t_h is the time of the last flux measurement to consider (d). Such a parameter allows quantitative comparison of N_2O emissions between samples and decreasing pressure head steps even when there are incomplete flux chronicles, i.e., without knowing the maximum flux of a step. Furthermore, this parameter is well adapted to the study of N_2O emissions dynamics because it combines the notions of time and flux intensity.

The effect of hydric cycles, sampling periods, pressure head steps, or treatments were assessed by a Mann–Whitney U test or a Kruskal–Wallis test at the 5% level. Correlations were assessed by the calculation of Spearman correlation coefficients. Both the means and their associated standard errors of means are reported.

3 Results

3.1 Soil physical and chemical properties

The average BD of the soil samples collected in January was a little but significantly lower than that of the samples collected in May ($p < 0.01$, Table 1). The modal pore diameter as determined by porosimetry analysis was in the range of 2.99 to 4.10 μm (Table 1). These small differences between soil samples on small aggregates led us to hypothesize that differences in the BD were caused by differences in the macroporosity. Total N and SOC at the sampling time were in the same order of magnitude in January and May but were slightly higher in May. This trend remained the same after the experiment on the tension table ($p < 0.05$, Table 1). There was no statistically significant difference in SOC or total N between treatments ($p > 0.05$). Before the experiments, the NO_3 content of the soil cores was in the same order of magnitude in January and May. At the end of the experiment, the soil NO_3 concentrations ranged between 28.5 and 84.0 mg N kg^{-1}, which confirms that NO_3 was supplied in excess (Table 1). No trend was observed between the final NO_3 concentration and the N_2O emissions, the sampling period, or the treatment applied ($p > 0.05$).

3.2 Hydric control

After the hanging water column was moved to a lower pressure head step, the soil matric potential decreased abruptly and then reached a plateau (Fig. 2). The time needed for the matric potential to reach the plateau was computed from tensiometer records (Table 3). The plateau was reached within approximately 5, 7, and 10 h after lowering the pressure head to −7, −25, and −50 cm, respectively, and was reached more rapidly during C2 than during C1 (not significant, $p > 0.05$). The 24-h increments between the pressure head steps were not always long enough for the matric potential to stabilize, especially for the −75 and −100 cm pressure head steps. The phase of steep decline in the matric potential was defined by fitting the best linear regression to the tensiometer records at the beginning of a pressure head step (mean $R^2 = 0.91$). The time of the end of this phase is reported in Table 3.

The mean WFPS values at the matric potential plateau were calculated for each wetting–drying cycle (Table 3). The WFPS was > 60% for all pressure head steps in the 0 to −100 cm range and throughout all of the cycles. The hydric conditions were thus favorable for denitrification (Grundmann and Rolston, 1987; Hénault and Germon, 2000). Moreover, for a given pressure head step, we did not find any significant difference in WFPS between

treatments ($p > 0.05$), which demonstrated a good reproducibility between experiments. No significant difference in WFPS was observed between the two cycles for a given pressure head step ($p > 0.05$); however, the WFPS appeared to be consistently lower during C2. This difference was equal to −3.2% WFPS at the 0 cm step and −1.1% WFPS at the −100 cm step. Although the experiment was designed to limit air entrapment by using an upward saturation, a small amount of hydric hysteresis occurred.

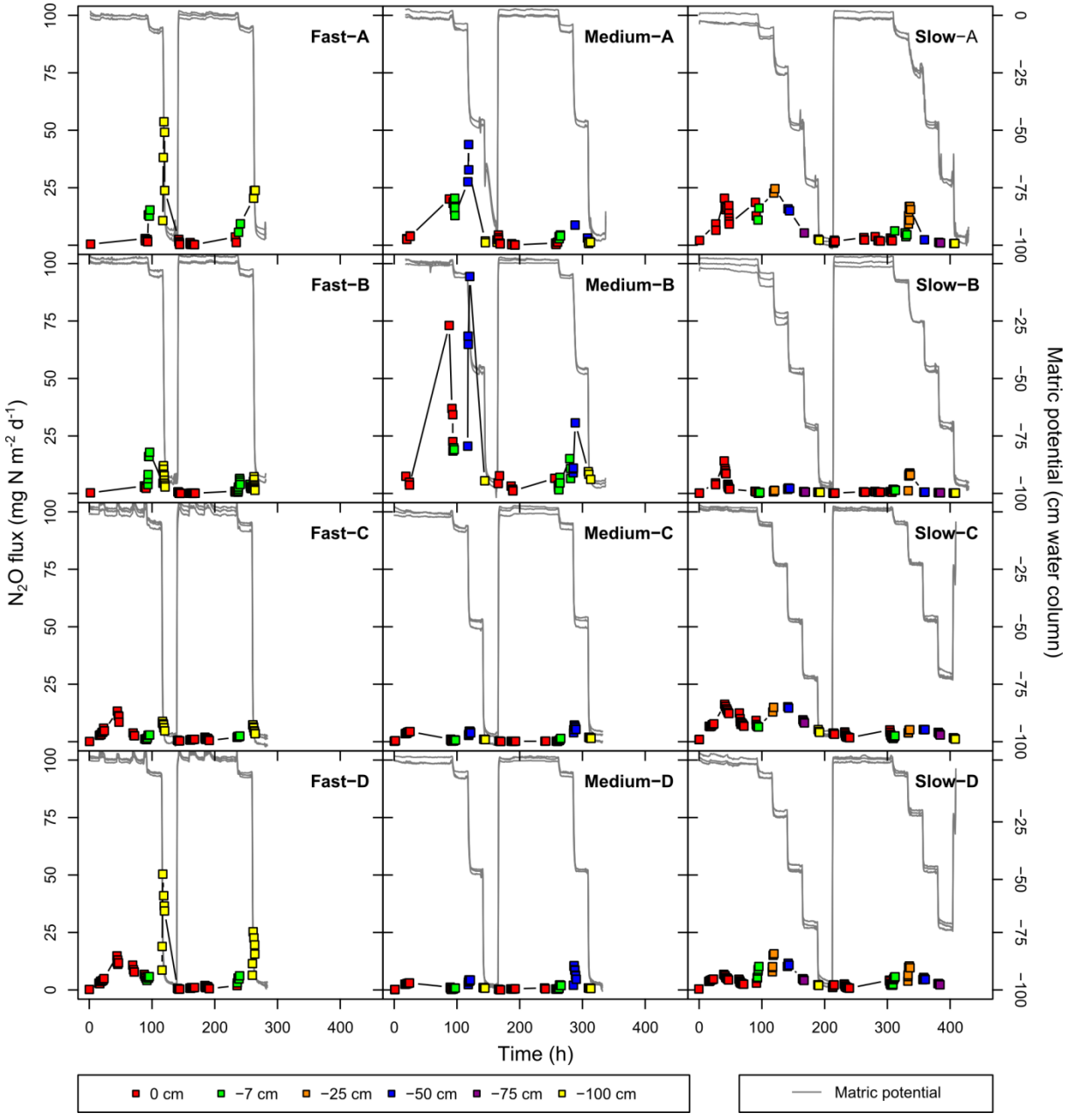

Fig. 2. Monitoring of the N_2O fluxes of the 12 soil samples and the soil matric potential by the three tensiometers (Fast: 3 values of decreasing pressure head, Medium: 4 values, Slow: 6 values). For the sake of readability, the measurement points are linearly interpolated.

Table 3. Evolution of the water-filled pore space (WFPS) and characterization of the soil matric potential dynamics (average ± standard error) at each pressure head step from 0 to −100 cm.

Cycle	0 cm (n = 12)	−7 cm (n = 12)	−25 cm (n = 4)	−50 cm (n = 8)	−75 cm (n = 4)	−100 cm (n = 12)
			WFPS, %			
C1	98.3 ± 1.5	88.4 ± 2.0	83.4 ± 2.3	80.3 ± 2.5	77.9 ± 2.3	76.6 ± 2.2
C2	95.1 ± 2.1	85.9 ± 2.4	81.0 ± 3.3	78.1 ± 2.2	75.9 ± 3.1	75.2 ± 2.5
			Time to reach equilibrium, h			
C1	–	6.1 ± 0.5	8.5 ± 1.3	11.2 ± 1.1	15.1 ± 2.7	15.4 ± 1.1
C2	–	5.1 ± 0.4	5.7 ± 0.7	9.3 ± 1.1	19.2 ± 1.8	15.8 ± 1.0
			End of the phase of steep decline in water potential, h			
C1	–	2.2 ± 0.2	1.1 ± 0.1	1.6 ± 0.3	1.2 ± 0.3	1.0 ± 0.1
C2	–	2.0 ± 0.1	2.5 ± 0.8	1.6 ± 0.3	0.9 ± 0.2	1.0 ± 0.1

3.3 Nitrous oxide emissions

The intensity of N_2O fluxes was highly variable among the sampling periods and among the treatments (Fig. 2). The mean cumulative N_2O fluxes were 63.1 ± 18.0 mg N m^{-2} d^{-1} for the Fast treatment, 100.1 ± 60.0 mg N m^{-2} d^{-1} for the Medium treatment, and 96.9 ± 25.2 mg N m^{-2} d^{-1} for the Slow treatment (not significant, $p > 0.05$). The lowest emissions were recorded for the Medium-C and Medium-D samples, whereas the highest emissions were recorded for the Medium-B sample.

Emissions were not monotonic with time and exhibited peaks induced by the pressure head steps (Fig. 2). Two types of N_2O peaks could be identified:

1. During the wetting phase (C1–0 or C2–0), the N_2O fluxes first increased slowly to reach a maximum and then decreased. For the Fast-D sample, for example, the N_2O fluxes increased from 0.2 to 14.8 mg N m^{-2} d^{-1} during 44 h after rewetting (P_{sat} peak) and then decreased to 5.1 mg N m^{-2} d^{-1} 90 h after the application of the pressure head (Fig. 3). The mean time for the peak to occur in all samples was 51.1 ± 21.7 h after rewetting.

2. During the drying phase, the N_2O fluxes first increased rapidly and then decreased. For the Fast-D sample, the N_2O fluxes at the −100 cm step reached a maximum only 1.2 h after the application of the pressure head at 50.4 mg N m^{-2} d^{-1}. They then decreased to 34.4 mg N m^{-2} d^{-1} at 3.9h after the application of the pressure head (Fig. 3). For all of the samples,

these P_{desat} peaks reached their maximum value within 1.6 ± 0.2 h after the pressure head was decreased. A linear relationship can be observed between the time of the maximum N_2O flux and the end of the phase of steep decline in the matric potential, taking into account all of the steps ($R = 0.61$, $p < 0.01$). The P_{desat} peaks were not observed in every pressure head step, especially the last pressure head steps of a cycle.

To analyze the data, we calculated the contribution of each step of the wetting–drying cycles on the total N_2O emissions by computing the *a* parameter (Eq. [2]). We did not find evidence of any effect of the sampling period ($p > 0.05$) for the C1–0 step, but a small effect appeared at the C1–7 step ($p = 0.05$). Emissions were significantly higher in January than in May. This difference is directly linked to the significantly higher BD at the second sampling period ($p < 0.01$): samples that had a BD that was > 1.33 g cm^{-3} showed a weaker N_2O flux slope (Fig. 4). However, this effect was not observed in the C2 cycle ($p > 0.05$).

Considering the first wetting–drying cycle, high N_2O fluxes were recorded during the wetting phase, but the N_2O flux slope was always low compared with some of the drying steps (e.g., at C1, 0.3 mg N m^{-2} d^{-2} during wetting and 8.3 mg N m^{-2} d^{-2} during drying for the highest P_{desat} peaks) (Fig. 5). For every sample, a peak of similar intensity was recorded at the −7 cm pressure head step across the range of 0.02 to 4.8 mg N m^{-2} d^{-2}. The highest P_{desat} peaks occurred during the pressure head step following the −7 cm pressure head step, i.e., step −100 cm for the Fast treatment, step −50 cm for the Medium treatment, and step −25 cm for the Slow treatment. The mean *a* parameter of these peaks was highly variable between samples: 12.0 ± 4.6 mg N m^{-2} d^{-2} for the Fast treatment, 11.0 ± 5.7 mg N m^{-2} d^{-2} for the Medium treatment, and 1.7 ± 0.8 mg N m^{-2} d^{-2} for the Slow treatment. The influence of the following steps became negligible after the highest P_{desat} peak was complete for all of the pressure heads applied ($p < 0.0001$ with the following steps).

By comparing the pressure head steps responsible for the highest P_{desat} peaks (i.e., step −100 cm for the Fast treatment, −50 cm for the Medium treatment, and −25 cm for the Slow treatment), we found a relationship with the volume of water drained after decreasing the pressure head ($R = 0.80$, $p < 0.05$) (Fig. 6). However, this effect was valid only if the N_2O flux was still high at the end of the wetting phase, as can be observed with the points that were sized according to the magnitude of the flux at the end of the saturation step in Fig. 6. It is also noteworthy that the N_2O flux slope was occasionally negative (Fig. 5), especially just after a P_{desat} peak.

The N_2O flux slopes showed similar patterns during C1 and C2 (Fig. 5), i.e., (i) little contribution during the wetting phase on the N_2O flux slope (C1–0 or C2–0), (ii) similar response between samples at the −7 cm pressure head step (C1–7 or C2–7), and (iii) highest P_{desat} peaks immediately after the −7 cm pressure head step. However, it is noteworthy that the fluxes were often lower during C2 than during C1 at the 0 cm step: the maximum fluxes were 7.5 ± 2.4 times lower at C2 than at C1, and the N_2O flux slope was equivalent to 0.30 ± 0.08 mg N m^{-2} d^{-2} at C1 and 0.03 ± 0.01 mg N m^{-2} d^{-2} at C2. For the −7 cm pressure head step, the trends were more complex: the N_2O flux slope tended to be higher in C2 when the outflow was higher in C2. The high variability observed between samples in C1 for the steps following the −7 cm pressure head step was reduced in C2, with N_2O flux slopes across the range 0.8 to 7.9 mg N m^{-2} d^{-2}, which is the same order of magnitude as the lowest N_2O flux slopes at C1. Additionally, the volume of water drained did not seem to affect the N_2O flux slope intensity at C2 (R = 0.27, p > 0.05).

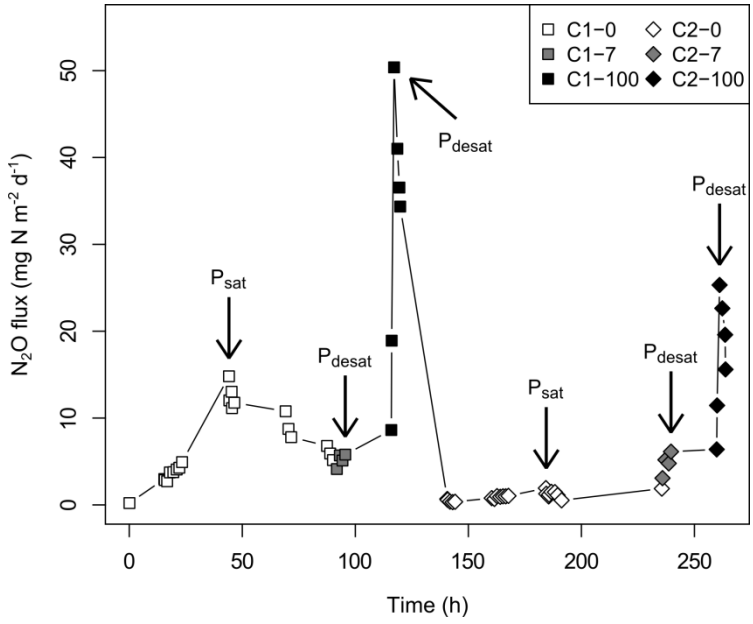

Fig. 3. Nitrous oxide fluxes with time of the Fast-D sample (squares and diamonds). Arrows indicate peak localization (P_{sat} is peak flux during the wetting phase, P_{desat} is peak flux during the drying phase; in the key, numbers refer to the negative pressure head applied in centimeters, C1 is the first cycle, C2 is the second cycle). For the sake of readability, the measurement points are linearly interpolated.

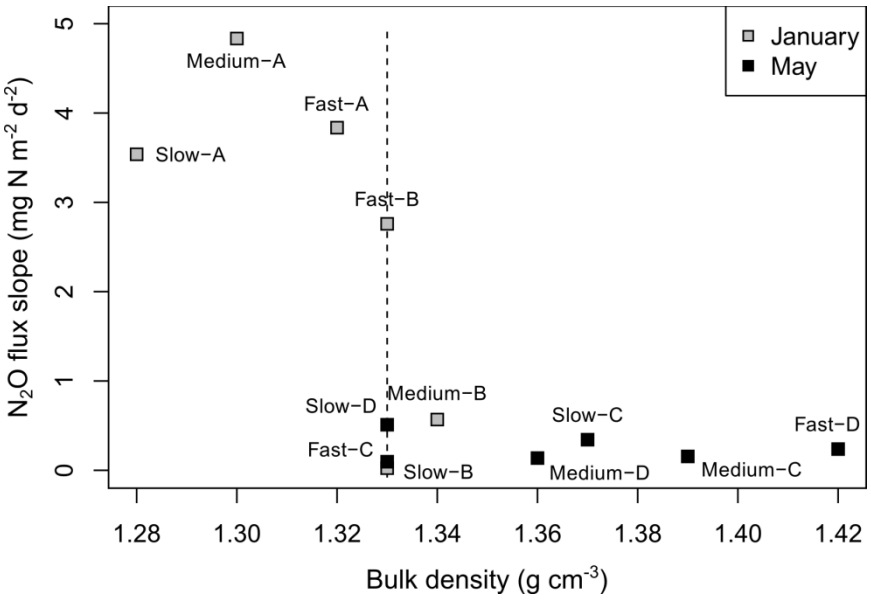

Fig. 4. Relationship between the N_2O flux slope and the bulk density at the −7 cm pressure head of the first wetting–drying cycle (Fast: 3 values of decreasing pressure head, Medium: 4 values, Slow: 6 values).

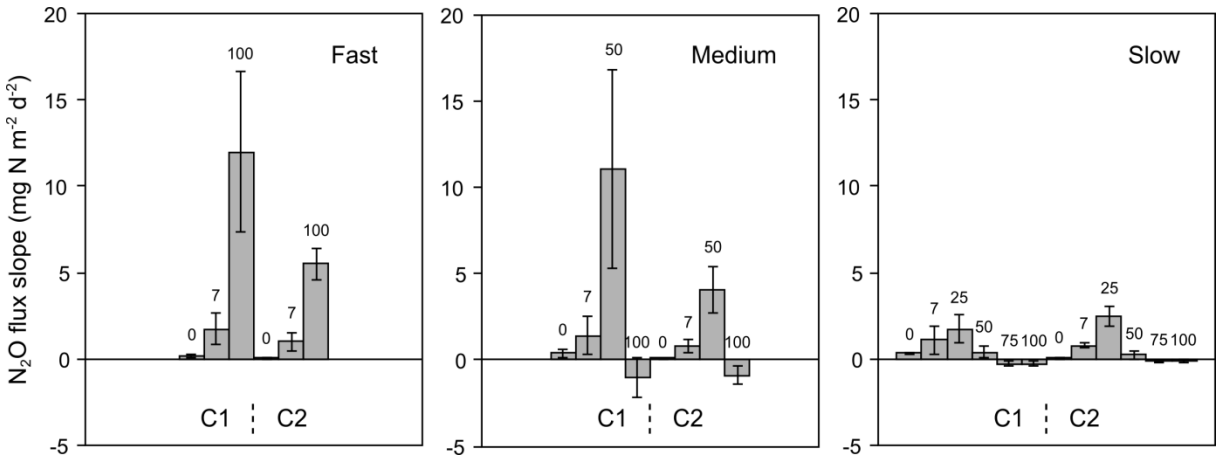

Fig. 5. Nitrous oxide flux slope from the initial moment of changing water potential according to the pressure head step (numbers refer to the negative pressure head applied in centimeters, C1 is the first cycle, C2 is the second cycle; Fast: 3 values of decreasing pressure head, Medium: 4 values, Slow: 6 values). Error bars represent standard errors.

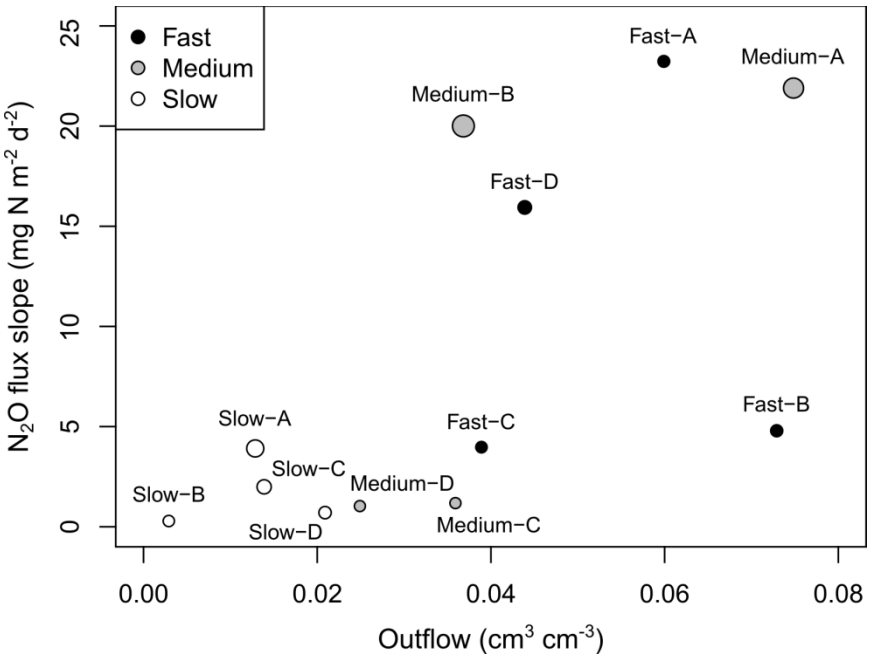

Fig. 6. Relationship between N_2O flux slope and the amount of water drained at the second step of the decreasing pressure head (Fast: −100 cm, Medium: −50 cm, Slow: −25 cm pressure head) of the first wetting–drying cycle. The points are proportional in size to the N_2O flux at the end of the wetting step.

4 Discussion

4.1 Discriminating the nitrous oxide peaks

Two types of N_2O peaks were observed. According to their width and the time lag after the hydric event, the peaks appear to represent two different processes. During the wetting phase to saturation, the P_{sat} peaks occurred within 2 to 3 d after wetting and could be attributed to microbial processes because denitrifying microorganisms gradually adapt to anaerobic conditions (Laville et al., 2011). This type of peak has often been captured in the field or laboratory soon after the rewetting of a soil (e.g., Groffman and Tiedje, 1988; Sanchez-Martin et al., 2010; Sexstone et al., 1985). In contrast, the P_{desat} peaks during the drying phase may be related to physical processes. These peaks occurred just after the decrease of the pressure head, when the shift in soil matric potential was the fastest. In this respect, a relationship has been observed between the time of the maximum N_2O flux and the end of the steep decline in the soil matric potential. The N_2O emissions could have originated from gas that was previously entrapped in pore space during the wetting phase. Nitrous oxide may also have been released from the soil solution as it moved to reach equilibrium. Nevertheless, this type

of experimental setup provides no indisputable evidence for the exact origin of the released N_2O, that is, from the gaseous or liquid phase. The two processes may have occurred at the same time.

Previous studies that sampled gas inside the soil or disrupting soil cores have reported that a large part of the N_2O was still entrapped in water-saturated soils after a short-term experiment (e.g., Weier et al., 1993; Wollersheim et al., 1987). Clough et al. (1999) observed that 7.4% of the ^{15}N-labeled NO_3 that was added at the beginning of their experiment was recovered entrapped in soil pores after 38 d and that 2% was dissolved in the soil solution, whereas < 1% was emitted as N_2O. Nitrous oxide emissions have already been observed by Huang et al. (2007) to be higher during natural drying than during wetting. They hypothesized that cracks formed at the soil surface raised the O_2 concentration, enhancing the N_2O emissions. Conversely, the soil solution was saturated with N_2O in their water-saturated soil sample.

4.2 The effect of drying intensity and drying history

Peaks of N_2O emissions were observed during the drying phase for all pressure head steps from −7 to −100 cm. From a quantitative point of view, the rate of N_2O released was related to the amount of water drained (Fig. 6). When the pressure head is decreased, the air–water interface withdraws to the bottom of the soil cylinder and exposes pores to the atmosphere as the water drains. For a large pressure head decrease, the finer pores are drained, therefore the volume concerned is large and gas emissions are important. In addition, the degassing of the dissolved N_2O is more likely to occur when large amounts of water are moved. Clough et al. (2000) already observed gas displacement into the soil after a hydric event: N_2O was displaced downward by the application of water to the soil surface. Castellano et al. (2010) found that the maximum N_2O flux rates occurred at a mean matric potential of −3.75 kPa for soils of different textures in their free drainage experiment. They concluded that peaks occurred when pores > 40 μm were drained. This is consistent with our findings, where the highest fluxes were observed from the −50 and −100 cm steps, equivalent to a maximum water-filled pore radius of approximately 60 and 30 μm, respectively. Castellano et al. (2010) concluded that the size of the water-filled pores was an important controlling factor of N_2O emissions. In our experiment, BD appeared to also be a determinant of the N_2O flux slope at the −7 cm step but not for higher steps. Indeed, at the −7 cm pressure head step, only pores > 420 μm were free of water. The water movements in these large pores during drainage favor

the equilibrium between the liquid and the gaseous phases according to Henry's law and therefore N_2O emission to the atmosphere. Moreover, gas diffusion through these macropores is favored for low BD because N_2O production microsites are more likely to be connected to the soil surface. At higher suction values, more gas pathways are available and the effect of BD is weaker. Therefore, the pore size distribution is important because macropores are involved in the gas transport, whereas the microbiological production of N_2O takes place in the water-filled micropores (Heincke and Kaupenjohann, 1999).

However, the fact that high fluxes did not last more than two drying steps and that the N_2O flux slope was sometimes negative suggests a reservoir-based functioning. Adopting the terms of Yoh et al. (1997), an active phase and a late phase may be distinguished. During the active phase, the production of N_2O by microorganisms is the major process that produces N_2O, and the poor gas diffusivity at high water content leads to the entrapment of a part of this N_2O in the soil in the gaseous or liquid phase. During the late phase, N_2O production is low and the major process is the release of the accumulated N_2O. However, whereas Yoh et al. (1997) stressed that the contribution of the late phase was of little importance because of the short residence time of N_2O in soils, our study demonstrates that it can be of major importance in the case of changing hydric equilibrium. In addition, in our experiments, the N_2O flux slope was recorded to be negative when the N_2O emissions returned to a baseline after a peak. This suggests that no additional entrapped gas existed. The N_2O flux to the soil surface is faster in a dry soil than in a wet soil; therefore, the production occurring during the drying phase can be easily released and is not likely to be entrapped. The total amounts of N_2O emissions were estimated by calculating the cumulative N_2O fluxes and were found to be in the same order of magnitude for the three treatments of decreasing pressure heads. Even if the different treatments affected the dynamics of N_2O emission (magnitude and speed), the same cannot be said for the total amounts of N_2O that were emitted. Therefore, it can be inferred that the soil drying, in the range that we applied, did not alter the production process differently in the three treatments.

The hydric history of the soil was also considered through the second wetting–drying cycle. During the wetting phase, the fluxes were less intense during C2 than during C1. A possible explanation arising from our experiment is that this trend may have been caused by the hydric hysteresis between the primary wetting–drying curve and the main wetting–drying curve of the soil water retention curve. Indeed, the second saturation of soil entraps air in such a way

that saturation cannot be complete (Kutílek and Nielsen, 1994). In our study, the WFPS fell by 3.2% between the C2–0 step and the C1–0 step; therefore anoxic conditions and N substrate supply were slightly reduced. A decrease in N mineralization in a second wetting–drying cycle has already been reported and was attributed to the disruption of microbial activity during the rise or decrease of the water potential, which can be seen as a hydric stress (Muhr et al., 2008). It has also been attributed to an increasing proportion of tolerant microorganisms or their adaptation to water stress, which reduced the microbial nutrient release (Fierer and Schimel, 2002; Mikha et al., 2005) and their metabolic capacities (Schimel et al., 2007). Other researchers have implicated a shortage of mineralizable C after a previous cycle of enhanced microbial activity (Fierer and Schimel, 2002). Furthermore, because the effect of the physical disruption of soil aggregates on the protection of organic matter is limited to few wetting and drying cycles (Denef et al., 2001), less C substrate would have been released during C2. Given the short duration of the experiment in the current study, no shortage of organic C was observed.

As previously noted, the N_2O production was lower during C2 than during C1, as observed with N_2O fluxes at the 0 cm step (Fig. 2). Therefore, during the drying phase, the N_2O flux slope could not be related to the amount of water drained at C2 using the same model as for C1. While the reservoir was filled with N_2O as in the C2–7 step, the relative contributions of C1 and C2 were linked to the relative amount of water drained: the N_2O flux slope was higher at C1 when the outflow was higher at C1. However, this trend cannot be transposed for the following drying steps because the amount of N_2O entrapped was limiting. In addition, the shorter time to reach the plateau near the hydric equilibrium at C2 provided a shorter window of opportunity to release N_2O.

4.3 A dynamic link between nitrous oxide fluxes and the water-filled pore space?

Under steady-state conditions, the values taken into account to build the WFPS–N_2O flux relationship are often maximum N_2O fluxes of soil samples at hydric equilibrium (e.g., Grundmann and Rolston, 1987; Hénault and Germon, 2000). Under these conditions, 60% WFPS is known to be favorable for N_2O emissions because the physical and biological conditions are considered to be suboptimal for nitrification and denitrification. Indeed, neither substrate diffusion nor O_2 diffusion is limiting (Bateman and Baggs, 2005). Micropores are water filled, promoting microbial activity, whereas macropores are air filled, allowing

efficient aeration of the soil (Davidson et al., 2000). Furthermore, the reduction of N_2O into N_2 is not likely to occur near 60% WFPS because N_2O reductase is inhibited by O_2 (Knowles, 1982). The observations in our present study could not reproduce such a simple relationship because the system was in a non-steady-state equilibrium. Therefore, the N_2O flux emissions measured at a given time depended on the previous hydric state.

From a dynamic point of view, we have demonstrated the need to link the water content and diffusion processes in addition to addressing aspects of N_2O production. Indeed, diffusion can be extremely lowered when a soil is water filled (De Wever et al., 2004; Thorbjørn et al., 2008). We therefore recommend using a gas diffusion model in addition to the static WFPS–N_2O relationship to estimate natural N_2O fluxes. In this respect, Yoh et al. (1997) successfully modeled N_2O fluxes from Fick's law and the estimated N_2O production rate. To quantify the impact of the deployment of a closed chamber on the measured fluxes, Venterea et al. (2009) and Conen and Smith (2000) also modeled N_2O diffusion from soil to a closed chamber by applying gas transport theory. Moreover, when the soil is unsaturated, solid-induced tortuosity and water-induced disconnectivity also affect the gas diffusion (Thorbjørn et al., 2008). Solid-induced tortuosity is an intrinsic parameter, depending on the soil texture and soil structure, whereas water-induced disconnectivity is governed by the water content and the direction of the change in water content (wetting or drying). Satisfying hydrostatic requirements, water and air are distributed into the soil to reach equilibrium. The water-filled pore diameter depends on the pore diameter, surface tension, and contact angle between the solid surface and water, according to the Jurin–Laplace law. This results in saturated portions of the porous network that can be disconnected from the air percolating network and would then constitute potential volumes of N_2O, either entrapped as gas pockets or dissolved in the liquid phase. The role of the porous network structure was taken into account by Laudone et al. (2011), who built a modeled pore network composed of macro- and micropores. They used Fickian diffusion corrected for the tortuosity of the microporosity to estimate diffusion from hotspots of biological activity.

Considering N_2O emissions as a dynamic mechanism ultimately requires taking into account three types of time-dependent processes: gradual or sequential processes (e.g., microbial growth, unsteady water flow, sequential biogeochemical reactions), time lags (e.g., storage and diffusion of gases into the soil), and indirect effects (e.g., cell lysis after rewetting the soil and the reuse of the released nutrients as substrate).

Our study highlights the role of the state of the hydric equilibrium of the soil on N_2O emissions, which may be responsible for the high temporal variability of N_2O fluxes observed in the field. The limited diffusion of gases in the soil when pores are water filled can lead to errors in flux calculations using the headspace method because steady-state conditions are never reached under field conditions (McCarty et al., 1999). Furthermore, because the change in water content is relatively fast after irrigation or rainfall, underestimations of N_2O fluxes may occur if peaks are not captured by a large gas sampling interval (Xing et al., 2011). Our study underscores the fact that N_2O peaks can occur with similar intensity during the wetting or drying phase, suggesting that field sampling should be performed at both of these two periods with a fine temporal resolution. Monitoring the water content, or better, the water potential, appears to be an indispensable aid in choosing the sampling period and its time interval and in explaining and modeling the trends that are observed.

Conclusions

In previous studies, the intensity of N_2O emissions and their evolution with time were often explained by microbial population dynamics that faced variations in environmental conditions. The experiments performed in this study were intended to demonstrate the additional role of soil water on N_2O emissions dynamics.

Nitrous oxide peaks appeared to be induced by changes in the matric potential. They were observed after both small (−7 cm water column) and more intense (−100 cm) drying events. The highest emissions were detected within the first two steps of the decreasing pressure head for all the treatments applied. Because the hydric conditions were favorable for N_2O emissions (WFPS > 60%) throughout the experiments, these highest emissions at the beginning of the drying phase could not be directly linked with the aerobic state of the soil, as is usually performed with the WFPS–N_2O flux exponential or Gaussian relationship. Entrapment of N_2O may have occurred during the wetting phase, and rapid displacement may have occurred during the drying phase. Two types of peaks were identified and were linked to different mechanisms: production during the wetting phase and release of the gas that was trapped in soil pores or dissolved in the soil solution. The intensities of the peaks during the drying phase were correlated with the amount of water drained in the first wetting–drying cycle and occurred during the steep decline of the soil matric potential, approximately 1 to 2 h after lowering the pressure head. This short interval can explain why this type of peak during the drying phase has not been described in previous studies.

The fact that the intensities of the N_2O peaks during the drying phase can be higher, although peaks last for less time, than those of the wetting phase, highlights the need to take into account the hydric history of soils and its physical processes in the understanding of N_2O emissions by soils.

Acknowledgments

We are grateful to D. Colosse, P. Courtemanche, and G. Giot for their technical help in the experimental design of this study. We also thank C. Le Lay for assistance in field sampling and A. Besnault and O. Josière for laboratory analysis. Carbon and nitrogen analyses were graciously performed by the SAS Laboratoire. This work was supported by a Conseil Général du Loiret grant, by the Spatioflux program funded by the Région Centre, FEDER, INRA and BRGM, and by the Labex VOLTAIRE (ANR-10-LABX-100-01).

References

Appel, T. 1998. Non-biomass soil organic N: The substrate for N mineralization flushes following soil drying–rewetting and for organic N rendered CaCl2–extractable upon soil drying. Soil Biol. Biochem. 30:1445–1456. doi:10.1016/S0038-0717(97)00230-7

Bateman, E.J., and E.M. Baggs. 2005. Contributions of nitrification and denitrification to N2O emissions from soils at different water-filled pore space. Biol. Fertil. Soils 41:379–388. doi:10.1007/s00374-005-0858-3

Beare, M.H., E.G. Gregorich, and P. St-Georges. 2009. Compaction effects on CO2 and N2O production during drying and rewetting of soil. Soil Biol. Biochem. 41:611–621. doi:10.1016/j.soilbio.2008.12.024

Birch, H.F. 1958. The effect of soil drying on humus decomposition and nitrogen availability. Plant Soil 10:9–31. doi:10.1007/BF01343734

Borken, W., and E. Matzner. 2009. Reappraisal of drying and wetting effects on C and N mineralization and fluxes in soils. Global Change Biol. 15:808–824. doi:10.1111/j.1365-2486.2008.01681.x

Castellano, M.J., J.P. Schmidt, J.P. Kaye, C. Walker, C.B. Graham, H. Lin, and C.J. Dell. 2010. Hydrological and biogeochemical controls on the timing and magnitude of

nitrous oxide flux across an agricultural landscape. Global Change Biol. 16:2711–2720. doi:10.1111/j.1365-2486.2009.02116.x

Ciarlo, E., M. Conti, N. Bartoloni, and G. Rubio. 2007. The effect of moisture on nitrous oxide emissions from soil and the N2O/(N2O + N2) ratio under laboratory conditions. Biol. Fertil. Soils 43:675–681. doi:10.1007/s00374-006-0147-9

Clough, T.J., S.C. Jarvis, E.R. Dixon, R.J. Stevens, R.J. Laughlin, and D.J. Hatch. 1999. Carbon induced subsoil denitrification of 15N-labelled nitrate in 1 m deep soil columns. Soil Biol. Biochem. 31:31–41. doi:10.1016/S0038-0717(98)00097-2

Clough, T.J., R.R. Sherlock, and K.C. Cameron. 2000. Entrapment and displacement of nitrous oxide in a drained pasture soil. Nutr. Cycling Agroecosyst. 57:191–193. doi:10.1023/A:1009891717386

Clough, T.J., R.R. Sherlock, and D.E. Rolston. 2005. A review of the movement and fate of N2O in the subsoil. Nutr. Cycling Agroecosyst. 72:3–11. doi:10.1007/s10705-004-7349-z

Conen, F., and K.A. Smith. 2000. An explanation of linear increases in gas concentration under closed chambers used to measure gas exchange between soil and the atmosphere. Eur. J. Soil Sci. 51:111–117. doi:10.1046/j.1365-2389.2000.00292.x

Davidson, E.A., M. Keller, H.E. Erickson, L.V. Verchot, and E. Veldkamp. 2000. Testing a conceptual model of soil emissions of nitrous and nitric oxides. BioScience 50:667–680. doi:10.1641/0006-3568(2000)050[0667:TACMOS]2.0.CO;2

Decagon Devices. 2010. 5TE water content, EC and temperature sensors: Operator's manual. Vol. 7. Decagon Devices, Pullman, WA.

Denef, K., J. Six, H. Bossuyt, S.D. Frey, E.T. Elliott, R. Merckx, and K. Paustian. 2001. Influence of dry–wet cycles on the interrelationship between aggregate, particulate organic matter, and microbial community dynamics. Soil Biol. Biochem. 33:1599–1611. doi:10.1016/S0038-0717(01)00076-1

Denman, K.L., G. Brasseur, A. Chidthaisong, P. Ciais, P.M. Cox, R.E. Dickinson, et al. 2007. Couplings between changes in the climate system and biogeochemistry. In: S. Solomon et al., editors, Climate change 2007: The physical science basis. Contribution

of Working Group I to the Fourth Assessment Report of the Intergovernmental Panel on Climate Change. Cambridge Univ. Press, Cambridge, UK.

De Wever, H., D.T. Strong, and R. Merckx. 2004. A system for studying the dynamics of gaseous emissions in response to changes in soil matric potential. Soil Sci. Soc. Am. J. 68:1242–1248. doi:10.2136/sssaj2004.1242

Dobbie, K.E., I.P. McTaggart, and K.A. Smith. 1999. Nitrous oxide emissions from intensive agricultural systems: Variations between crops and seasons, key driving variables, and mean emission factors. J. Geophys. Res. 104(D21):26891–26899. doi:10.1029/1999JD900378

Fierer, N., and J.P. Schimel. 2002. Effects of drying–rewetting frequency on soil carbon and nitrogen transformations. Soil Biol. Biochem. 34:777–787. doi:10.1016/S0038-0717(02)00007-X

Groffman, P.M., K. Butterbach-Bahl, R.W. Fulweiler, A.J. Gold, J.L. Morse, E.K. Stander, et al. 2009. Challenges to incorporating spatially and temporally explicit phenomena (hotspots and hot moments) in denitrification models. Biogeochemistry 93:49–77. doi:10.1007/s10533-008-9277-5

Groffman, P.M., and J.M. Tiedje. 1988. Denitrification hysteresis during wetting and drying cycles in soil. Soil Sci. Soc. Am. J. 52:1626–1629. doi:10.2136/sssaj1988.03615995005200060022x

Grundmann, G.L., and D.E. Rolston. 1987. A water function approximation to degree of anaerobiosis associated with denitrification. Soil Sci. 144:437–441. doi:10.1097/00010694-198712000-00008

Gu, J.X., B. Nicoullaud, P. Rochette, D.J. Pennock, C. Hénault, P. Cellier, and G. Richard. 2011. Effect of topography on nitrous oxide emissions from winter wheat fields in central France. Environ. Pollut. 159:3149–3155. doi:10.1016/j.envpol.2011.04.009

Heincke, M., and M. Kaupenjohann. 1999. Effects of soil solution on the dynamics of N2O emissions: A review. Nutr. Cycling Agroecosyst. 55:133–157. doi:10.1023/A:1009842011599

Heinen, M. 2006. Simplified denitrification models: Overview and properties. Geoderma 133:444–463. doi:10.1016/j.geoderma.2005.06.010

Hénault, C., and J.C. Germon. 2000. NEMIS, a predictive model of denitrification on the field scale. Eur. J. Soil Sci. 51:257–270. doi:10.1046/j.1365-2389.2000.00314.x

Huang, S.H., H.K. Pant, and J. Lu. 2007. Effects of water regimes on nitrous oxide emission from soils. Ecol. Eng. 31:9–15. doi:10.1016/j.ecoleng.2007.04.001

Khalil, M.A.K., R.A. Rasmussen, and M.J. Shearer. 2002. Atmospheric nitrous oxide: Patterns of global change during recent decades and centuries. Chemosphere 47:807–821. doi:10.1016/S0045-6535(01)00297-1

Kieft, T.L., E. Soroker, and M.K. Firestone. 1987. Microbial biomass response to a rapid increase in water potential when dry soil is wetted. Soil Biol. Biochem. 19:119–126. doi:10.1016/0038-0717(87)90070-8

Knowles, R. 1982. Denitrification. Microbiol. Rev. 46:43–70.

Kroeckel, L., and H. Stolp. 1986. Influence of the water regime on denitrification and aerobic respiration in soil. Biol. Fertil. Soils 2:15–21. doi:10.1007/BF00638956

Kutílek, M., and D.R. Nielsen. 1994. Soil hydrology. Catena Verlag, Cremlingen-Destedt, Germany.

Laudone, G.M., G.P. Matthews, N.R.A. Bird, W.R. Whalley, L.M. Cardenas, and A.S. Gregory. 2011. A model to predict the effects of soil structure on denitrification and N2O emission. J. Hydrol. 409:283–290. doi:10.1016/j.jhydrol.2011.08.026

Laville, P., S. Lehuger, B. Loubet, F. Chaumartin, and P. Cellier. 2011. Effect of management, climate and soil conditions on N2O and NO emissions from an arable crop rotation using high temporal resolution measurements. Agric. For. Meteorol. 151:228–240. doi:10.1016/j.agrformet.2010.10.008

Linn, D.M., and J.W. Doran. 1984. Effect of water-filled pore space on carbon dioxide and nitrous oxide production in tilled and nontilled soils. Soil Sci. Soc. Am. J. 48:1267–1272. doi:10.2136/sssaj1984.03615995004800060013x

Mathieu, O., C. Hénault, J. Lévêque, E. Baujard, M.J. Milloux, and F. Andreux. 2006. Quantifying the contribution of nitrification and denitrification to the nitrous oxide flux using 15N tracers. Environ. Pollut. 144:933–940. doi:10.1016/j.envpol.2006.02.005

McCarty, G.W., D.R. Shelton, and A.M. Sadeghi. 1999. Influence of air porosity on distribution of gases in soil under assay for denitrification. Biol. Fertil. Soils 30:173–178. doi:10.1007/s003740050605

Mikha, M.M., C.W. Rice, and G.A. Milliken. 2005. Carbon and nitrogen mineralization as affected by drying and wetting cycles. Soil Biol. Biochem. 37:339–347. doi:10.1016/j.soilbio.2004.08.003

Muhr, J., S.D. Goldberg, W. Borken, and G. Gebauer. 2008. Repeated drying–rewetting cycles and their effects on the emission of CO2, N2O, NO, and CH4 in a forest soil. J. Plant Nutr. Soil Sci. 171:719–728. doi:10.1002/jpln.200700302

Ravishankara, A.R., J.S. Daniel, and R.W. Portmann. 2009. Nitrous oxide (N2O): The dominant ozone-depleting substance emitted in the 21st century. Science 326:123–125. doi:10.1126/science.1176985

Sanchez-Martin, L., A. Sanz-Cobena, A. Meijide, M. Quemada, and A. Vallejo. 2010. The importance of the fallow period for N2O and CH4 fluxes and nitrate leaching in a Mediterranean irrigated agroecosystem. Eur. J. Soil Sci. 61:710–720. doi:10.1111/j.1365-2389.2010.01278.x

Schimel, J., T.C. Balser, and M. Wallenstein. 2007. Microbial stress-response physiology and its implications for ecosystem function. Ecology 88:1386–1394. doi:10.1890/06-0219

Sexstone, A.J., T.B. Parkin, and J.M. Tiedje. 1985. Temporal response of soil denitrification rates to rainfall and irrigation. Soil Sci. Soc. Am. J. 49:99–103. doi:10.2136/sssaj1985.03615995004900010020x

Stark, J.M., and M.K. Firestone. 1995. Mechanisms for soil moisture effects on activity of nitrifying bacteria. Appl. Environ. Microbiol. 61:218–221.

Thorbjørn, A., P. Moldrup, H. Blendstrup, T. Komatsu, and D.E. Rolston. 2008. A gas diffusivity model based on air-, solid-, and water-phase resistance in variably saturated soil. Vadose Zone J. 7:1276–1286. doi:10.2136/vzj2008.0023

van Gestel, M., J.N. Ladd, and M. Amato. 1991. Carbon and nitrogen mineralization from two soils of contrasting texture and microaggregate stability: Influence of sequential fumigation, drying and storage. Soil Biol. Biochem. 23:313–322. doi:10.1016/0038-0717(91)90185-M

Venterea, R.T., K.A. Spokas, and J.M. Baker. 2009. Accuracy and precision analysis of chamber-based nitrous oxide gas flux estimates. Soil Sci. Soc. Am. J. 73:1087–1093. doi:10.2136/sssaj2008.0307

Weier, K.L., J.W. Doran, J.F. Power, and D.T. Walters. 1993. Denitrification and the dinitrogen/nitrous oxide ratio as affected by soil water, available carbon, and nitrate. Soil Sci. Soc. Am. J. 57:66–72. doi:10.2136/sssaj1993.03615995005700010013x

Wollersheim, R., G. Trolldenier, and H. Beringer. 1987. Effect of bulk density and soil water tension on denitrification in the rhizosphere of spring wheat (Triticum vulgare). Biol. Fertil. Soils 5:181–187.

World Meteorological Organization. 2007. Scientific assessment of ozone depletion, 2006. Global Ozone Res. Monit. Project Rep. 50. World Meteorol. Organ., Geneva.

Wuebbles, D.J. 2009. Nitrous oxide: No laughing matter. Science 326:56–57. doi:10.1126/science.1179571

Xing, H.T., E.L. Wang, C.J. Smith, D. Rolston, and Q. Yu. 2011. Modelling nitrous oxide and carbon dioxide emission from soil in an incubation experiment. Geoderma 167–168:328–339. doi:10.1016/j.geoderma.2011.07.003

Yoh, M., H. Toda, K. Kanda, and H. Tsuruta. 1997. Diffusion analysis of N2O cycling in a fertilized soil. Nutr. Cycling Agroecosyst. 49:29–33. doi:10.1023/A:1009757829417